HAL
open science

Multi-level filtering segmentation to measure individual tree parameters based on Lidar data: Application to a mountainous forest with heterogeneous stands

C. Véga, Sylvie Durrieu

To cite this version:

C. Véga, Sylvie Durrieu. Multi-level filtering segmentation to measure individual tree parameters based on Lidar data: Application to a mountainous forest with heterogeneous stands. International Journal of Applied Earth Observation and Geoinformation, 2011, 13 (4), p. 646 - p. 656. 10.1016/j.jag.2011.04.002 . hal-00634844

HAL Id: hal-00634844

https://hal.science/hal-00634844v1

Submitted on 24 Oct 2011

HAL is a multi-disciplinary open access archive for the deposit and dissemination of scientific research documents, whether they are published or not. The documents may come from teaching and research institutions in France or abroad, or from public or private research centers.

L'archive ouverte pluridisciplinaire **HAL**, est destinée au dépôt et à la diffusion de documents scientifiques de niveau recherche, publiés ou non, émanant des établissements d'enseignement et de recherche français ou étrangers, des laboratoires publics ou privés.

Author-produced version of the article published in International Journal of Applied Earth Observation and Geoinformation, 2011, 13(4), 646-656.
The original publication is available at http://www.elsevier.com
DOI: 10.1016/j.jag.2011.04.002

*Manuscript
Click here to view linked References

Multi-level filtering segmentation to measure individual tree parameters based on Lidar data: application to a mountainous forest with heterogeneous stands.

Cédric Véga (1)*, Sylvie Durrieu (2)

UMR TETIS Cemagref-Cirad-ENGREF

Maison de la Télédétection en Languedoc-Roussillon

500, rue J.F. Breton BP 5095

34196 Montpellier Cedex 05

FRANCE

* corresponding author

(1): cedric.vega@teledetection.fr, Tel. 00 33 (0) 4 67 54 87 19

(2): sylvie.durieu@teledetection.fr, Tel. 00 33 (0) 4 67 54 87 32

Fax: 00 33 (0) 4 67 54 87 00

Author-produced version of the article published in International Journal of Applied Earth Observation and Geoinformation, 2011, 13(4), 646-656.
The original publication is available at http://www.elsevier.com
DOI: 10.1016/j.jag.2011.04.002

Abstract

This paper presents a method for individual tree crown extraction and characterisation from a Canopy Surface Model (CSM). The method is based on a conventional algorithm used for localising LM on a smoothed version of the CSM and subsequently for modelling the tree crowns around each maximum at the plot level. The novelty of the approach **lies** in the introduction of controls on both the degree of CSM **filtering** and the shape of elliptic crowns, in addition to a multi-**filtering level** crown fusion approach to balance omission and commission errors. The algorithm derives the total tree height and the mean crown diameter from the elliptic tree crowns generated. The method was tested and validated on a mountainous forested area mainly covered by mature and even-aged black pine (*Pinus nigra* ssp. *nigra* [Arn.]) stands. Mean stem detection per plot, using this method, was 73.97 %. Algorithm performance was affected slightly by both stand density and heterogeneity (i.e. tree diameter classes' distribution). The total tree height and the mean crown diameter were estimated with root mean squared error values of 1.83 m and 1.48 m respectively. Tree heights were slightly underestimated in flat areas and overestimated on slopes. The average crown diameter was underestimated by 17.46 % on average.

Keywords : lidar, airborne laser scanning; mountainous forests, tree extraction, canopy surface model

Author-produced version of the article published in International Journal of Applied Earth Observation and Geoinformation, 2011, 13(4), 646-656.
The original publication is available at http://www.elsevier.com
DOI: 10.1016/j.jag.2011.04.002

Introduction

Acquiring detailed information on tree spatial distribution and tree crown characteristics is a crucial step when attempting to improve our understanding of the structure and function of forest ecosystems and to ensure their sustainable development. Traditional field-based inventories require time-consuming and labour-intensive work that can only be applicable to small areas (Avery and Burkhart, 2001). With the development of very high resolution remote sensing, single tree crowns can be identified, thus enabling an automatic extraction of some tree characteristics at operational scales (Leckie et al., 2005).

Scanning laser altimetry or lidar (light detection and ranging) generates detailed and accurate information about forest 3D structure (Means et al., 2000; Popescu et al., 2003), and is used at an operational level in some coniferous forests (Næsset et al., 2004). Lidar systems combine a micropulse laser unit, a Global Positioning Systems (GPS) and Inertial Measurement Units (IMU) to produce high precision measurements of the Earth surface structure (Baltsavias, 1999). Due to the ability of the signal to partially penetrate canopies, lidar measurements, acquired as 3D point clouds or waveforms, can be used to produce detailed information on both ground topography and vegetation layer (Reutebush et al., 2003). In the last decades high density lidar data - at least 5 points by squared meter (Næsset, 2004) – were successfully used to retrieve forest parameters at the tree level including tree location, tree height, crown dimensions, tree biomass and even the tree species (Brandtberg, 2007; Popescu, 2007; Rowell et al., 2006; Solberg et al., 2006). Such high densities are

Author-produced version of the article published in International Journal of Applied Earth Observation and Geoinformation, 2011, 13(4), 646-656.
The original publication is available at http://www.elsevier.com
DOI: 10.1016/j.jag.2011.04.002

required to describe the crown area in adequate detail (Hyyppä et al., 2001) and to increase the rate of tree apices effectively sampled (Leckie et al., 2003).

Methods for deriving individual tree parameters from lidar data mainly rely on the processing of a canopy surface model (CSM) describing the outer canopy layer (Bongers, 2001). They were commonly based on techniques applied for the processing of optical imagery (Leckie et al., 2003; Falkowski et al., 2008). Widely used approaches are based on geometrical properties (i.e. height, slope, orientation) of CSMs and mainly consist in the identification of local maxima (LM) followed by the construction of crown segments (Morsdorff et al., 2004; Persson et al., 2002; Popescu et al., 2002).

The accuracy of automated tree detection relies heavily on image spatial resolution (see Pouliot and King (2005) for review). Several methods were introduced to optimize LM identification i.e. to minimize either the level of commission (i.e. false tree detection) or omission errors. These include conventional image filtering (Persson et al., 2002), height-based variable window size filtering (Popescu et al., 2004) or template matching (Brandtberg et al., 2003). Approaches used to extract segments from the set of LM include; watershed analysis (Kwak et al., 2007; Mei and Durrieu, 2004), region growing algorithms (Hyyppä et al., 2001; Persson et al., 2002), fitting functions (Popescu et al., 2002) or template matching (Pollock, 1996). As methods for deriving crown characteristics are mostly based on CSM geometry, the resulting crown shapes are directly impacted by the CSM optimization strategy (Rowell et al., 2006; Solberg et al., 2006).

Author-produced version of the article published in International Journal of Applied Earth Observation and Geoinformation, 2011, 13(4), 646-656.
The original publication is available at http://www.elsevier.com
DOI: 10.1016/j.jag.2011.04.002

On the whole, both LM detection and crown modelling approaches reveal high sensitivity to initial parameters (Pouliot and King, 2005) and optimisations are generally performed on a field knowledge basis, which hinders direct **extendibility** to different forest ecosystems (Popescu et al., 2002; Koch et al., 2006). While methods have been introduced to evaluate the reliability of either the LM or the crown segments (Brandtberg et al., 2003; Rowell et al., 2006; Solberg et al., 2006) more generic and flexible approaches need to be developed to satisfactorily manage various forest types and structures.

This paper presents a **multi-level filtering** approach to extract and characterise individual tree crown parameters from a lidar CSM. The segmentation is based on the extraction of LM and on the modelling of tree crown using ellipsis defined using the local geometrical properties of the CSM surrounding each LM. The method integrates algorithms to control both the degree of CSM filtering and tree crown shape, and to merge tree crown segments derived at various scales. **In order to evaluate the extendibility potential of the method the** study was conducted within **a complex environment**, a mountainous conifer forests characterized by steep slopes and diverse stand structures and densities.

1. Material

1.1. Study area

The study site (Fig. 1) is a 108 ha area that was reforested at the end of the **19**th century. It is located in the southern French Alps, to the north of Digne-les-Bains (Alpes de Haute

Author-produced version of the article published in International Journal of Applied Earth Observation and Geoinformation, 2011, 13(4), 646-656.
The original publication is available at http://www.elsevier.com
DOI: 10.1016/j.jag.2011.04.002

Provence) and is part of an Observatory for Research on the Environment (ORE) dedicated to the monitoring of erosion and hydrological processes in mountainous areas. The site is mainly covered by mature and even-aged black pine (*Pinus nigra ssp. nigra* [Arn.]) stands growing at elevations ranging between 802 m and 1 263 m. The mean slope is about 53 % but can locally reach up to 100 %. The whole forest is currently subject to intensive management (selective cutting) to renew the forest and to contribute to the regeneration of native species. These activities have a direct impact on the forest mosaic characterized by varying stand structures.

[Insert Fig. 1 about here]

1.2. Field data

Field inventory data were collected during December 2007 (**14 plots**) and November 2008 (**13 plots**). The plots (**N=27**) were established to represent the whole range of stand conditions and were inventoried according to the French National Forest Inventory protocol (NFI, http://www.ifn.fr). Each plot comprised 3 concentric rings of 6, 9 and 15 m radius from the plot centre, in which trees to be inventoried were selected based on their diameter at breast height (dbh). Within the 6 m radius plot, all the trees having a dbh greater than 7.48 m were considered. The minimum dbh **values were set to** 22.44 cm and 34.7 cm respectively for the second (6-9 m) and the third (9-15m) rings. For each tree considered, the dbh, the total timber height, and the tree state (dead or alive) were recorded. The protocol was slightly modified for 2 plots characterized by gentle slopes. All the trees having a dbh greater than 7.48 m were inventoried and additional measurements were collected for the crown diameter

Author-produced version of the article published in International Journal of Applied Earth Observation and Geoinformation, 2011, 13(4), 646-656.
The original publication is available at http://www.elsevier.com
DOI: 10.1016/j.jag.2011.04.002

(measurements taken in North-South and Est-West directions). **Such limited crown measurements were established considering (1) the time available for field measurements, (2) the difficulty to have reliable field crown measurements on slope terrains and (3) the possibility to have a visual control of crown delineation quality using high resolution images complementary to field measurements.**

The structural diversity of the plot was estimated using the Gini diversity index (Lexerød and Eid, 2006, Ozdemir et al., 2008). The Gini coefficient (*GC*) was calculated as follows:

$$GC = \sum_{j=1}^{n} (2j-n-1)ba_j \Big/ \sum_{j=1}^{n} ba_j(n-1) \qquad (1)$$

where j is the rank of a tree according to size in ascending order, n is the total number of trees and ba_j the basal area for tree j. *GC* values are inside the [0-1] interval. A value of 0 indicates that all trees in a given area have exactly the same diameter. On the other hand, a value of 1 characterises forest areas in which each tree has a unique dbh value.

The exact plot centre positions were measured using differential GPS (DGPS) or a Leica total station (Leica, Switzerland) whenever the local slope conditions permitted this. Individual tree positions were derived from distance and angle measurements taken from the plot centre. Distance measurements were made at the tree base using a Vertex III clinometer (Hagloff, Sueden) with slope compensation. Azimuths and tree heights were measured using a Suunto compass (Suunto, Finland). Measurements of crown diameters and trunk circumference at breast height were performed using tapes. The dbh were derived from trunk circumferences. Due to low DGPS accuracy (around 2 m) within the area, the plot centre positions were

Author-produced version of the article published in International Journal of Applied Earth Observation and Geoinformation, 2011, 13(4), 646-656.
The original publication is available at http://www.elsevier.com
DOI: 10.1016/j.jag.2011.04.002

visually corrected in the laboratory by visually matching tree location with photo-interpreted tree crowns on the lidar data. Two plots were discarded because of insufficient positional accuracy **and the impossibility to obtain a satisfactory matching within the close neighbourhood**.

[Insert Table 1 about here]

In addition, a topographic survey was conducted in May 2009 to validate the quality of the lidar ground elevation model. Four forested plots located in areas with different topographical conditions were surveyed, comprising a total of 891 ground control points. Additional 502 points were collected in open areas leading to a total number $\mathbf{N_{GCP}}$ **of 1393. Measurements** were made using a Leica total station.

1.3. Lidar data acquisition and processing

The lidar data were acquired by Sintegra (Grenoble, France) in April 2007 using a RIEGL LMS-Q560 instrument (Wagner et al., 2006). This small footprint fullwaveform airborne laser scanner operates at a pulse frequency of 111 kHz. The sampling was performed at about 600 m above ground level leading to a mean footprint diameter of 0.25 m at the ground level. A 30 % overlap was set between adjacent flight lines to avoid slivers (Latipov, 2002). Point density obtained was close to 5.5 pts / m^2.

Waveform processing was performed using RiAnalyze © solftware from Riegl (Riegl, Austria) based on a Gaussian pulse estimation technique. The method combines the rapid

Author-produced version of the article published in International Journal of Applied Earth Observation and Geoinformation, 2011, 13(4), 646-656.
The original publication is available at http://www.elsevier.com
DOI: 10.1016/j.jag.2011.04.002

calculation of the gravity centre of the echo pulse with the accuracy of a multiple Gaussian pulse fitting method (Riegl, 2007). During this processing step a set of 3D points are derived from the waveforms, describing the position of targets having interacted with the laser signal (Chauve et al., 2009).

The resulting point cloud was classified as vegetation or ground elements to create a DTM and a CSM representing the shape of the canopy surface. To match the average point spacing, the DTM and the CSM were computed at 1 m and 0.5 m resolutions respectively.

The points corresponding to the ground level were extracted by the data provider from the last returns using a TIN-iterative algorithm (Axelsson, 2000) applied with Terrascan software (Terrasolid, http://www.terrasolid.fi/en/products/terrascan). The resulting Triangulated Irregular Network was then converted into a 1 m cell grid.

The "non-ground" returns were interpolated into a Digital Surface Model (DSM) using a two-step method. First, the point cloud was converted into a regular grid with a 0.5 m resolution using neighbouring statistics. Each DSM cell was assigned the maximum height value of the points within it. The Inverse Distance Weighting (IDW) method was used to compute empty cell values by interpolating the point values selected at the previous stage. A CSM at a 0.5 m spatial resolution was finally calculated by subtracting the DTM from the DSM.

2. Methods

Author-produced version of the article published in International Journal of Applied Earth Observation and Geoinformation, 2011, 13(4), 646-656.
The original publication is available at http://www.elsevier.com
DOI: 10.1016/j.jag.2011.04.002

2.1. General principle of the method

The method we propose to extract individual tree crowns is based on conventional algorithms used to locate LM on a smoothed version of the CSM and to subsequently model the tree crowns around each maximum at the plot level (Fig. 2, Segmentation box). The segmentation included the following 5 steps: 1) Hole-filling 2) Gaussian filtering of the CSM_{HF}, 3) Extraction of LM, 4) Modelling of elliptic crown shapes, 5) Cleaning of LM and corresponding crowns. The latter step involved filtering out LM and corresponding crowns to keep a single LM per crown (priority given to the LM associated with the largest crown) (see section 3.3.4).

The novelty of the approach **lies** in the introduction of i) **a hole filling algorithm to locally improve the CSM quality**, ii) a threshold-based method to control the degree of CSM **filtering**, ii) a control of the shape of elliptic crowns and iii) a multi-**level filtering** crown fusion to balance omission and commission errors (Fig. 2).

[Inset Fig. 2 about here]

2.2. Hole-filling algorithm

Lidar CSMs are commonly beset by pit problems due to both lidar sampling design and post-processing of the raw data including point classification and interpolation (Ben-Aries et al., 2009). We developed a straightforward and automatic algorithm to improve both CSM

Author-produced version of the article published in International Journal of Applied Earth Observation and Geoinformation, 2011, 13(4), 646-656.
The original publication is available at http://www.elsevier.com
DOI: 10.1016/j.jag.2011.04.002

filtering quality and segmentation accuracy (either with or without CSM filtering). We opted for this solution instead of the semi-automated method proposed by Ben-Aries et al. (2009) as it would have been more complex to parameterize.

The algorithm first calculates if a given pixel value is lower than a given threshold (fixed to 0.5 m here) compared to its 8-connected pixels. If the condition is fulfilled, the pixel tested value is replaced by the mean value of its 8 neighbours. Otherwise, the algorithm tests if the condition could by fulfilled using 4-connected pixels (vertical cross, oblique cross). This meant that holes of more than 1 pixel were filled. Again, if a neighbouring configuration matched the height condition, the tested pixel value is replaced by the corresponding mean value of those 4 connected pixels. The algorithm iterates until no pixel value is modified. This hole-filled CSM (CSM_{HF}) was used as a starting point for the segmentation process (Fig. 2).

2.3. Segmentation method

The algorithm was coded using Python 2.4 (http://www.python.org/) with Numpy 1.2.1 (http://www.scipy.org/) and the ArcGIS 9.2 geoprocessing tools (www.esri.com/).

2.3.1. Filtering of the CSM_{HF}

The CSM_{HF} was smoothed using a Gaussian low-pass 3 × 3 filter (Hyyppä et al., 2001). The filter weights were 1/4 for the central pixel, 1/8 for the 4 nearest pixels (Y and Y direction)

Author-produced version of the article published in International Journal of Applied Earth Observation and Geoinformation, 2011, 13(4), 646-656.
The original publication is available at http://www.elsevier.com
DOI: 10.1016/j.jag.2011.04.002

and 1/16 for the diagonal ones. The number of Gaussian runs was optimized for every plot according to a user defined threshold (see section 3.5.1).

2.3.2. Locating local maxima

LMs were created by extracting the centre coordinates of pixels having a higher height value than their 8 connected neighbours. Only the LMs above 3 m in height were considered.

2.3.3. Extracting elliptic tree crowns

Tree crowns around each LM were modelled as ellipsis. The algorithm was based on the measurement of the crown size in the 8 cardinal directions. The measurements were made downwards from the LM, starting from each of the 8 pixels connected to the LM. For any given direction, a pixel was considered as part of the crown if, and only if, its height value and those of two of its neighbours were lower than the last connected pixel fulfilling that condition. The position of the two "constraining" neighbours was set depending on the tested direction as illustrated in Fig. 3. An additional constraint was set to fix the minimum height of the crown outer limit. A 2 m threshold was used for trees exceeding 10 m, and a threshold of 0.5 m otherwise. Such very similar thresholds were set to accurately model tree crowns in open areas and to improve calculation efficiency. The number of pixels composing a crown radius was then translated into distance based on pixel size.

The condition for including a point within a crown radius was relaxed when no Gaussian filtering was used (i.e. iteration 1) to balance the effect of noise within the CSM_{HF}. To

Author-produced version of the article published in International Journal of Applied Earth Observation and Geoinformation, 2011, 13(4), 646-656.
The original publication is available at http://www.elsevier.com
DOI: 10.1016/j.jag.2011.04.002

include a point within the crown radius measurement, only one out of the two constraining pixels must fulfil the height condition ("or" criteria instead of "and").

[Insert Fig. 3 about here]

As the accuracy of crown radius measurement may vary depending on the local structure of the CSM, the 8 measured radii of a crown were compared to identify **suspicious** measurements and to retain the most reliable ones for the elliptic crown shape computation. First, the crown diameters were computed for the four directions (N-S; E-W; NE-SW; NW-SE) by adding the corresponding crown radii. Then, the radii corresponding to orthogonal diameters having the smallest distance difference were selected as master radii of the crown ellipse. Finally, the four remaining radii values were individually compared to their two encircling master ones. If the tested radius was within the interval of the mean of the two encircling master radii ± twice their standard deviation (SD), then it was integrated within the ellipse definition. Otherwise, the radius was removed. At the end of the process, 4 to 8 radii remained and were used to define the ellipse approximating the crown.

Such elliptic representations of tree crown shapes were obtained by 1) converting the radii into points representing the outer limit of the crown using distance and angle measurement from the LM coordinates and 2) applying a standard deviational ellipse algorithm to the resulting point cloud provided within the ArcGis spatial Analyst toolbox (http://webhelp.esri.com/).

2.3.4. Cleaning of local maxima and corresponding crowns

Author-produced version of the article published in International Journal of Applied Earth Observation and Geoinformation, 2011, 13(4), 646-656.
The original publication is available at http://www.elsevier.com
DOI: 10.1016/j.jag.2011.04.002

Depending on the spatial arrangement of LMs the elliptic crowns associated with each LM may partially overlap. The algorithm authorized crown overlapping under the condition that overlapping areas did not included any LM (i.e. a LM could only be inside a unique crown). The later rule lies on the hypothesis that a LM falling within the crown of a neighbouring LM may be a false apex detection. Each LM located within at least 2 crowns were tested and false apex detection were set for LM whose corresponding crown had a lower area than the other considered crowns. Therefore, the cleaning step consisted in removing such identified LM and their corresponding crown. Note that only the crowns having at least a 5 m^2 area were considered. Such a threshold was set according to field data and visual analysis of the CSM.

2.4. Estimating tree parameters

The algorithm recorded the crown area as well as the height of the tree. The latter is defined as the maximum height of the original CSM within the crown.

2.5. Optimisation of the segmentation

2.5.1. Controlling the degree of CSM filtering

This step relies on the hypothesis that there is a specific CSM_{HF} **filtering** degree at which the balance between omission and commission errors would be optimized. **Such an optimal filtering degree is expected to vary according to the both the plot structure and the**

Author-produced version of the article published in International Journal of Applied Earth Observation and Geoinformation, 2011, 13(4), 646-656.
The original publication is available at http://www.elsevier.com
DOI: 10.1016/j.jag.2011.04.002

canopy texture. In the present study, these later parameters were controlled introducing to empirically defined parameters hereafter refereed to as "structural parameter" and "segmentation parameter".

The "structural parameter" was used to assess the plot structure. It lies on the hypothesis that the relation between the number of extracted LM and the filtering intensity is closely related to the plot structure. In the present study, the "structural parameter" was defined as the rate of LM suppression between the number of extracted LM using 0 and 1 iteration of the Gaussian filter. As illustrated in Fig. 4, such a parameter was found to be a good estimator of the plot density of homogeneous stands (plot having at least 75% of stems in a same dbh class). Threshold values of 80 and 70 were used to classify plots within three structural classes according to the point clusters (Fig. 4).

The "segmentation parameter" was introduced to measure the proportion of noise within a set of identified LM and was calculated after each segmentation iteration as the ratio between the number of LM remaining after the cleaning step (step 5 of the segmentation process) and the number of LM **before the cleaning** step. **Such a parameter lies on the hypothesis that above a particular threshold value, the selected set of LM offers a good approximation of the spatial structure of dominant trees within a given area**. For example, a segmentation parameter **threshold set to a** value of 0.9 implied that 90 % of the extracted LM had to be converted into tree apices to reach the optimal number of Gaussian run. **The threshold values were estimated for each structural class based on a trial-error** experiment using 20 randomly selected plots. In the present study, values of 0.98, 0.90 and

Author-produced version of the article published in International Journal of Applied Earth Observation and Geoinformation, 2011, 13(4), 646-656.
The original publication is available at http://www.elsevier.com
DOI: 10.1016/j.jag.2011.04.002

0.80 were used respectively for high, medium and low values of the structural parameter, as illustrated on Table 2.

Note that the minimum number of Gaussian runs was set at 1, and the maximum to 6 according to Solberg et al. (2006) and to experimental results.

[Insert Table 2 about here]

2.5.2. Multi-level filtering crown fusion

The multi-***level*** **filtering** crown fusion approach was introduced to improve segmentation results, considering that the ideal **filtering** level of the CSM would vary depending on the crown size distribution within a given area. **Filtering** the CSM_{HF} with an increasing number of Gaussian runs tends to progressively improve segmentation results on dominant tree crowns to the detriment of the smaller ones. Such an effect may dominate within heterogeneous stands leading to underestimation of plot density.

To balance this effect, **some of the** crowns extracted using lower Gaussian filtering levels **and stored within temporary data bases**, were reintroduced, in descending filtering order, to make up the final set of tree crowns. Only crowns, whose corresponding LM were not inside the existing set of crowns, were added.

Author-produced version of the article published in International Journal of Applied Earth Observation and Geoinformation, 2011, 13(4), 646-656.
The original publication is available at http://www.elsevier.com
DOI: 10.1016/j.jag.2011.04.002

2.6. Statistical analysis

The modelled tree crowns were matched with their corresponding ground measured trees according to tree location and height. If more than one field-measured tree position was found in a modelled crown, the tree having the highest height was considered.

Due to the presence of a significant amount of leaning trees on the field, a certain proportion of modelled crowns could not be easily paired with any field-measured tree. In such cases, the modelled crowns were associated with their closest field-measured tree provided that the latter was not already associated to a crown. Otherwise the modelled crown was deemed a false detection.

Statistical analysis involved estimating the proportion of omission and commission errors at the plot level. Because of the specificities of the NFI plots, the analysis was **made** for each tree size category (small, medium and large diameters). For the matched trees, the accuracy of CSM derived tree heights and, **when field measurements were available, of crown diameters**, were assessed by calculating the mean difference and the root mean squared error (RMSE) of the difference **between field and lidar derived measurements**. Further investigations were carried out to account for both plot structure and terrain slope characteristics.

3. Results and Discussion

Author-produced version of the article published in International Journal of Applied Earth Observation and Geoinformation, 2011, 13(4), 646-656.
The original publication is available at http://www.elsevier.com
DOI: 10.1016/j.jag.2011.04.002

3.1. DTM and Hole-filled CSM quality

DTM quality was assessed using the 1393 ground control points. Over open areas (mainly roads), the average difference between field and lidar (i.e. field minus lidar) data was - 0.05 m (± 0.36 m SD). The minimum and maximum error values were - 0.57 and 4.77 m respectively. Over forested areas (N =891), the average difference was 0.24 m (± 0.81 m SD), minimum and maximum values were -2.88 and 4.22 m respectively. The plot-level DTM error increased as a function of slope from 0.02 m (± 0.3 m SD) to 0.65 m (±0.86 m SD) for plot-averaged mean slopes of 59.42 % and 86.03 %. Such increased slope related errors were explained by the difficulties involved in filtering algorithms to work within rough and forested terrain due to the underlying assumption regarding the bare Earth structure in a local neighbourhood (Sithole and Vosselman, 2004). These errors were also caused by issues linked to algorithm parameter optimisation over large and topographically complex areas (Kobler et al., 2007). Underestimation of terrain elevation over a slope may be explained by the propensity of TIN-iterative methods to be influenced by low points. A detailed discussion on filtering algorithms limitations and possible ways of improving them is available in Sithole and Vosselman (2004).

Fig. 5 illustrated the results of the hole-filing algorithm. The resulting CSM_{HF} was only qualitatively evaluated through visual comparison with the original CSM. As expected, pits localized within tree crowns were mostly removed while gaps between trees were well preserved. Such characteristics are required prior to CSM **filtering** and for extracting trees crowns (Rowell et al., 2006).

Author-produced version of the article published in International Journal of Applied Earth Observation and Geoinformation, 2011, 13(4), 646-656.
The original publication is available at http://www.elsevier.com
DOI: 10.1016/j.jag.2011.04.002

[Insert Fig. 5 about here]

3.2. Tree detection

The segmentation results are illustrated Fig. 6 for three plots having different densities and slopes. The optimal number of Gaussian runs was found to range from 1 (i.e. the minimal authorized value) to 4 with an average value of 1.8 (± 0.96 SD) (Table 3). **Half of the plots (52 %) were segmented using a unique Gaussian filter, 20 % needed two filtering iterations and another 20% 3 iterations. The remaining plots were segmented using 4 Gaussian filters**. From all the identified tree stems by plots, 90.3 % of the crowns were obtained from the CSM smoothed with the optimized number of Gaussian filter runs. The multi-level **filtering** crown fusion approach to crown detection generated about **10 %** of overall results, thus, emphasizing how important it is to consider multiple **filtering** levels when refining tree crown detection as underlined by Rowell et al. (2006). **According to the plot the contribution of crowns derived from lower filtering level varied from 0 to 50% of the total number of extracted crowns.**

[Insert Table 3 about here]

[Insert Fig. 6 about here]

Overall, the performance of the algorithm correlated with plot density, the latter parameter explaining 64 % of result variance (Fig. 7). Up to 800 stem/ha, segmentation accuracy was superior to 90 % for 9 plots over 11 and was obtained with significant **filtering** efforts (i.e. 2 to 4 Gaussian runs) (Fig. 7) which meant that the density and crown dimensions were

Author-produced version of the article published in International Journal of Applied Earth Observation and Geoinformation, 2011, 13(4), 646-656.
The original publication is available at http://www.elsevier.com
DOI: 10.1016/j.jag.2011.04.002

correctly modelled (Fig. 6A). With increasing plot densities, the number of Gaussian filters tended to decrease to efficiently match plot structure. Similarly, Rowell et al. (2006) reported both an overestimation of stem count without **filtering** in low density and thinned plots, and an underestimation of stem count with **filtering** in dense ones.

The general decrease in segmentation accuracy observed with increasing plot density was expected because high plot densities often lead to higher crown closure, the appearance of merged crowns that are difficult to isolate, and an increasing proportion of overtopped trees (Koch et al. 2006, Rowell et al. 2006, Solberg et al., 2006). However, by considering the performance of the algorithm by diameter classes, the rates of correctly identified tree crowns were respectively 98.18 % (±6,03 % SD), 92.63% (±11.61 % SD) and 45.66 % (±34,41% SD) for large, medium and small diameter classes (Table 3). The high percentage of trees identified for both large and medium diameter classes underline the utility of the method for management purposes. Indeed forest managers are particularly interested in the estimation of dominant and codominant tree crowns (Koch et al., 2006). Finally, while most of the non detection of tree crowns was due to overtopping, a proportion of error may be attributed to the 5 squared meter threshold used to define an ellipse as a tree crown. However this threshold level was retained, as experimental results gave an increased number of commission errors when using lower values.

Despite generally satisfactory performance, the algorithm produced inconsistent results for some plots characterized by variable densities and structural characteristics as reflected by the *GC* values **ploted as labels on Fig. 7**. These results concern poorly textured canopies (i.e. canopy with fused or/and relatively flat crowns). Within such plots, the structural parameter failed to optimize the number of filtering iterations, leading to over filtering of the CSM_{HF} and under-segmentation of the tree crowns that could not be counterbalanced by

Author-produced version of the article published in International Journal of Applied Earth Observation and Geoinformation, 2011, 13(4), 646-656.
The original publication is available at http://www.elsevier.com
DOI: 10.1016/j.jag.2011.04.002

multi-level **filtering** crown fusion **(see for example Fig. 6 D)**. Similar underestimations due to low height variance and poor CSM texture were found for different forests structures and types (Koch et al., 2006; Kwak et al., 2007). **In the present study, such poor results can be attributed to a failure to optimize the filtering process and might be mostly explained by the underlying hypothesis of the "segmentation parameter" regarding the modelling of dominant tree crowns. This weakness of the method could be over passed by introducing approaches** using fully textural indices to control the degree of **filtering** of the CSM_{HF}, e.g. indices derived either from wavelets transforms (Falkowski et al., 2006) or textural ordination based on Fourier spectral decomposition (Couteron et al., 2006), as both methods can be used to approximate crown size distribution. **In the same way, texture-based segmentation approaches such as the one proposed by Lucieer and Stein (2005) may also improve the robustness of the method by both minimizing effects of plot local structure on the optimization process and extending the method from the plot to the stand level.**

[Insert Table 4 about here]

[Insert Fig. 7 about here]

3.3. Height and crown characteristics

Tree heights were evaluated for 245 stems (Table 5). Lidar tree heights were on average 0.84 m (± 1.63 m SD) above the field measurements. Minimum and maximum absolute

Author-produced version of the article published in International Journal of Applied Earth Observation and Geoinformation, 2011, 13(4), 646-656.
The original publication is available at http://www.elsevier.com
DOI: 10.1016/j.jag.2011.04.002

differences were 0 m and 8.26 m respectively. The RMSE was 1.83 m. Overall the linear relationship accounted for 94 % of the total variance (Fig. 8).

Average difference was found to increase slightly with diameter, but converse results were found for standard deviation (Table 5). Nevertheless, height errors were closely correlated with slope.

A 0.1 m (± 0.65 m SD) tree height underestimation was found for terrain slopes lower than 25 %. The RMSE was 0.65 m. Such an underestimation was reported in most previous studies (Persson et al., 2002; Næsset and Økland, 2002) and was explained both by the discrete nature of the lidar sampling – increased density resulted in a higher proportion of sampled tree apices (Næsset and Økland, 2002) – and a partial penetration of the lidar signal within the canopy before a return could be detected by the lidar receiver (Gaveau and Hill, 2003).

Tree heights were overestimated for the 3 other terrain slope classes. Average values were respectively 0.18 m (± 0.65 m), 0.83 m (± 1.31 m SD) and 1.58 m (± 0.65 m SD) for [25 – 50 %[, [50 – 75 %[, and [75 - ∞] terrain slope classes. Corresponding RMSE were 0.97 m, 1.54 m and 2.5 m respectively. Similar results were reported in other studies related to mountainous environments (Hollaus et al., 2006; Takahashi et al. 2005). Heurich et al. (2003) suggested that lidar-derived tree height measurements must be corrected above 20° terrain slopes (e.g. 36.4 %). Such overestimations may be explained by several factors. One source of tree height overestimation may be attributed to DTM errors. As reported in section 4.1, DTM error differences around 0.7 m were found between roads and steep wooded areas. DTM underestimation contributed significantly to tree height measurement errors for steep terrain. Another source of tree height overestimation may be explained by a difference between field and lidar tree heights. In the field, tree height was defined as the vertical

Author-produced version of the article published in International Journal of Applied Earth Observation and Geoinformation, 2011, 13(4), 646-656.
The original publication is available at http://www.elsevier.com
DOI: 10.1016/j.jag.2011.04.002

distance from the tree apex to the upslope root crown (Fig. 9). The lidar-derived tree heights were simply calculated as the maximum value of the CSM within the crown area. Such calculation differences may lead to tree height overestimations for slopes as indicated by Takahashi et al. (2005). A 1 m horizontal difference between the tree apex and the tree base within a 100 % terrain slope produces a 1 m error in height measurement. Heurich et al. (2003) also pointed out that increased leaning trees and/or steeper terrain slopes generated increased systematic tree height errors.

[Insert Table 5 about here]

[Insert Fig. 8 about here]

Quality of crown diameter estimations was evaluated for 53 trees (Table 6). The plots were located in gentle terrain slopes having average values of 6 % (plot 1, Fig. 6A) and 13 % (plot 2, Fig. 6B). Plot densities were respectively 313 and 746 stem/ha for plot 1 ($\mathbf{N_{Crown}}$ = 13) and 2 ($\mathbf{N_{Crown}}$ = 40).

Plot 1 was segmented using a CSM_{HF} obtained after 3 Gaussian runs against a unique one for plot 2. Overall, lidar-derived values underestimated field measurements by 0.95 m (± 1.14 m SD) representing 17.45 % of the field measured values. Minimum and maximum values were -2.08 m and 6.02 m respectively. The 1.48 m RMSE was of the same range as mentioned in Popescu et al. (2003), which reported a 1.36 m RMSE for dominant trees of various pine trees species using a similar method. The Pearson correlation between field and lidar derived values was r = 0.63.

Author-produced version of the article published in International Journal of Applied Earth Observation and Geoinformation, 2011, 13(4), 646-656.
The original publication is available at http://www.elsevier.com
DOI: 10.1016/j.jag.2011.04.002

The error measurement increased slightly with density. While plot 1 showed a 0.79 m (± 1.14 m SD, 12.34%) mean underestimation, it reached 1 m (± 1.21 m SD, 19.11%) for plot 2. A **asymmetry** was also found when considering measurement direction (Table 6). The underestimation may be explained by both the field measurement strategy and the plot structure. In mountainous areas tree crowns are often dissymmetric and characterized by long branches exceeding the crown that may lead to an overestimation of the crown diameter. With increasing densities, the spatial arrangement of trees can generate a high level of merged crowns (Maier et al., 2008). Such characteristics could not be efficiently modelled using CSM geometrical properties. The reported varying error levels as a function of measurement direction highlight the impact of plot structure on crown measurement accuracy. The more compact a set of crown is, the greater the individual crown underestimation. Possible ways of improvements may include the use of more sophisticated filtering methods as suggested by Koch et al. (2006).

[Insert Table 6 about here]

[Insert Fig. 9 about here]

4. Conclusion

This research presents a method for extracting tree crown parameters from a lidar CSM acquired over mountainous areas. The method was based on conventional algorithms used to detect tree apices and model crown shape. The novelty of the approach **lies** in 1) **the**

Author-produced version of the article published in International Journal of Applied Earth Observation and Geoinformation, 2011, 13(4), 646-656.
The original publication is available at http://www.elsevier.com
DOI: 10.1016/j.jag.2011.04.002

introduction of a hole-filling algorithm to improve the initial CSM quality, 2) the optimization of the CSM filtering via the introduction of 2 parameters to quantitatively evaluate the plot spatial structure, 3) the introduction of a control method to optimize the shape of the identified tree crowns and 4) the application of a multi-level **filtering** crown fusion approach to improve the performance of the algorithm. The method performed quite well for most plots but failed to optimize filtering for some plots due to the complex structure or spatial organisation of the latter. **This was partly due to the fact that the optimization procedure was based on the presupposed behaviour of the identified dominant tree number when Gaussian iteration number increases. To account for this problem** future developments will focus on textural indices to improve both the description of the forest structure at the stand level and the robustness of the filtering process. **Taking into account the variability of the forest structure within the study site, we are confident that the method can be used in various forests conditions. However in very dense even aged young stands the canopy height patterns will probably not allow a correct crown segmentation, even with very high lidar point density, since intra-crown height variations can be for some species similar to inter-crown ones**. Furthermore, this research confirms some inconsistencies in height and crown width measurement regarding terrain slope and vegetation density. This issue would be addressed in future work dedicated to producing robust models of forest parameters and to improving management strategies within mountainous environments.

Acknowledgements

Author-produced version of the article published in International Journal of Applied Earth Observation and Geoinformation, 2011, 13(4), 646-656.
The original publication is available at http://www.elsevier.com
DOI: 10.1016/j.jag.2011.04.002

The authors would like to thank Laurent Albrech and Tristan Allouis for their valuable help in field data collection and post-processing. This work is part of the ExFOLIO project and was realized thanks to the financial support of the CNES (Centre National d'Etudes Spatiales). The authors would also like to deeply thank the GIS Draix for providing the full-waveform lidar data and for helping in ground truth surveys. They are grateful to INSU for its support to GIS Draix through the ORE program.

References

Avery, T.E., Burkhartn H.E., 2001. Forest measurements, 5th edn. McGraw–Hill, Boston.

Axelsson, P., 2000. DEM generation from laser scanner data using adaptative tin models. Int. Arch. Photogramm. Remote Sens.33, 110–117.

Baltsavias, E.P., 1999. Airborne laser scanning: basis relations and formulas ISPRS J. Photogramm. Remote Sens. 54, 199-214.

Ben-Arie, J.R., Hay, G.J., Powers, R.P., Castilla, G.,St-Onge, B., 2009. Development of a pit filling algorithm for LiDAR canopy height models. Comput. Geosci.35, 1940-1949.

Brandtberg, T.,Warner, T.A., Landenberger, R.E., McGraw, J.B., 2003. Detection and analysis of individual leaf-off tree crowns in small footprint, high sampling density lidar data from the eastern deciduous forest in North America. Remote Sens. Environ. 85, 290-303.

Author-produced version of the article published in International Journal of Applied Earth Observation and Geoinformation, 2011, 13(4), 646-656.
The original publication is available at http://www.elsevier.com
DOI: 10.1016/j.jag.2011.04.002

Brandtberg, T., 2007. Classifying individual tree species under leaf-off and leaf-on conditions using airborne lidar. ISPRS J. Photogramm. Remote Sens. 61, 325-340.

Bongers, F., 2001. Methods to assess tropical rain forest canopy structure: an overview. Plant Ecol. 153, 263–277.

Chauve, A., Véga, C., Durrieu, S., Bretar, F., Allouis, T., Pierrot Deseilligny, M., Puech, W., 2009. Processing full-waveform lidar data in an alpine coniferous forest: assessing terrain and tree height quality. Int. J. Remote Sens. 30, 5211-5228.

Couteron, P., Barbier, N., Gautier, D., 2006. Textural ordination based on Fourier spectral decomposition: a method to analyze and compare landscape patterns. Landscape Ecol. 21, 555–567.

Falkowski, M.J., Smith, A.M.S., Gessler, P.E., Hudak, A.T., Vierling, L.A., Evans, J.S., 2008. The influence of conifer forest canopy cover on the accuracy of two individual tree measurement algorithms using lidar data. Can. J. Rem. Sens. 34, S338-S350.

Gaveau, D.L.A., Hill, R.A., 2003. Quantifying canopy height underestimation by laser pulse penetration in small-footprint airborne laser scanning data. Can. J. Rem. Sens. 29, 650-657.

Heurich, M., Schneider, T., Kennel, E., 2003. Laser scanning for identification of forest structures in the Bavarian Forest National Park. Proceedings of ScandLaser, 2–4 September, Umeå, Sweden, pp. 97–106.

Author-produced version of the article published in International Journal of Applied Earth Observation and Geoinformation, 2011, 13(4), 646-656.
The original publication is available at http://www.elsevier.com
DOI: 10.1016/j.jag.2011.04.002

Hollaus, M., Wagner, W., Eberhofer, C., Karel, W., 2006. Accuracy of large-scale canopy heights derived from LiDAR data under operational constraints in a complex alpine environment. ISPRS J. Photogramm. Remote Sens. 60, 323-338.

Hyyppä, J., Kelle, O., Lehikoinen, M., Inkinen, M., 2001. A segmentation-based method to retrieve stem volume estimates from 3-D tree height models produced by laser scanners. IEEE Trans. Geosci. Remote Sens. 39, 969-975.

Kobler, A., N. Pfeifer, Ogrinc, P., Todorovski, L., Ostir, K., Dzeroski, S., 2007. Repetitive interpolation: A robust algorithm for DTM generation from Aerial Laser Scanner Data in forested terrain. Remote Sens. Environ. 108, 9-23.

Koch, B., Heyder, U., Weinacker, H., 2006. Detection of individual tree crowns in airborne lidar data. Photogramm. Eng. Remote Sens. 72(4), 357–363.

Kwak, D.-H., Lee, W.-K., Lee, J.H., Biging, G.S., Gong, P., 2007. Detection of individual trees and estimation of tree height using LiDAR data. J. For. Res. 12, 425–434.

Latypov, D., 2002. Estimating relative lidar accuracy information from overlapping flight lines. ISPRS J. Photogramm. Remote Sens. 56(4), 236-245.

Author-produced version of the article published in International Journal of Applied Earth Observation and Geoinformation, 2011, 13(4), 646-656.
The original publication is available at http://www.elsevier.com
DOI: 10.1016/j.jag.2011.04.002

Leckie, D.G., Gougeon, F.A., Tinis, S., Nelson, T., Burnet, C.N., Paradine, D., 2005. Automated tree recognition in old growth conifer stands with high resolution digital imagery. Remote Sens. Environ. 94, 311-326.

Leckie, D.G., Gougeon, F.A., Walsworth, N., Paradine, D., 2003. Stand delineation and composition estimation using semi-automated individual tree crown analysis. Remote Sens. Environ. 85, 355-369.

Lexerod, N.L., Eid, T., 2006. An evaluation of different diameter diversity indices based on criteria related to forest management planning. Forest Ecol. Manag. 222, 17-28.

Lucieer, A.,Stein, A., 2005. Texture-based landform segmentation of LiDAR imagery. Int. J. Appl. Earth Obs. Geoinf. 6(3-4), 261-270.

Maier, B., Tiede, D., Dorren, L., 2008. Characterising mountain forest structure using landscape metrics on LiDAR-based canopy surface models, in Blaschke, T., Lang, S., Hay, G.J. (Eds), Object-Based Image Analysis. Springer, Berlin, pp. 625-643.

Means, J.E., Acker, S.A., Fitt, B.J., Renslow, M., Emerson, L, Hendric, C.J., 2000. Predicting forest stand characteristics with airborne scanning Lidar. Photogramm. Eng. Remote Sens. 66, 1367-1371.

Mei, C., Durrieu, S., 2004. Tree-crown delineation from digital elevation models and high resolution imagery. Proceedings of the International Archives of the Photogrammetry,

Author-produced version of the article published in International Journal of Applied Earth Observation and Geoinformation, 2011, 13(4), 646-656.
The original publication is available at http://www.elsevier.com
DOI: 10.1016/j.jag.2011.04.002

Remote Sensing and Spatial Information Sciences 36, working group VIII/2, Laser-Scanners for Forest and Landscape Assessment. Freiburg, Germany.

Morsdorf, F., Meier, E., Kötz, B., Itten, K., Bobbertin, M., Allgöwer, B., 2004. LIDAR-based geometric reconstruction of boreal type forest stands at single tree level for forest and wildland fire management. Remote Sens. Environ. 92, 353-362.

Næsset, E., Gobakken, T., Holmgren, J., Hyyppä, H., Hyyppä, J., Maltano, M., Nilsson, M., Olsson, H., Persson, Ä., Söderman, U., 2004. Laser scanning of forest resources: the nordic experience. Scand. J. For. Res. 19, 482-499.

Næsset, E., Ökland, T., 2002. Estimating tree height and tree crown properties using airborne scanning laser in a boreal nature reserve. Remote Sens. Environ. 79, 105-115.

Næsset, E. 2004. Effects of different flying altitudes on biophysical stands properties estimated from canopy height and density measured with a small-footprint airborne scanning laser. Remote Sens. Environ. 91, 243-255.

Ozdemir, I., Norton, D.A.,Ozkan, U.Y., Mert, A., Senturk, O., 2008. Estimation of Tree Size Diversity Using Object Oriented Texture Analysis and Aster Imagery. Sensors 8, 4709-4724.

Persson, A., Holmgren, J., Söderman, U., 2002. Detecting and measuring individual trees using an airborne laser scanner. Photogramm. Eng. Remote Sens. 68, 925–932.

Author-produced version of the article published in International Journal of Applied Earth Observation and Geoinformation, 2011, 13(4), 646-656.
The original publication is available at http://www.elsevier.com
DOI: 10.1016/j.jag.2011.04.002

Pollock, R. 1996. The automatic recognition of individual trees in aerial images of forest based on a synthetic tree crown model. Vancouver, Canada: Ph.D. Thesis, Dept of Computer Science. University of British Columbia, 172 p.

Popescu, S.C., Wynne, R.H., Scrivani, J.A., 2004. Fusion of small-footprint lidar and multispectral data to estimate plot-level volume and biomass in deciduous and pine forests in Virginia, USA. For. Sci. 50, 551-565.

Popescu, S.C.,Wynne, R.H., Nelson, R.F., 2003. Measuring individual tree crown diameter with lidar and assessing its influence on estimating forest volume and biomass. Can. J. Rem. Sens. 29, 564-577.

Popescu, S.C.,Wynne, R.H., Nelson, R.F., 2002. Estimating plot-level tree heights with lidar: local filtering with a canopy-height based variable window size. Comput. Electron. Agric. 37, 1-95.

Popescu, S.C., 2007. Estimating biomass of individual pine trees using airborne lidar. Biomass Bioenerg. 31, 646-655.

Pouliot D., King, D., 2005. Approaches for optimal automated individual tree crown detection in regenerating coniferous forests. Can. J. Rem. Sens., 31(3): 255-267.

Author-produced version of the article published in International Journal of Applied Earth Observation and Geoinformation, 2011, 13(4), 646-656.
The original publication is available at http://www.elsevier.com
DOI: 10.1016/j.jag.2011.04.002

Reutebuch, S.E., McGaughey, R.J., Andersen, H.E., Carson, W.W., 2003. Accuracy of a high-resolution lidar terrain model under a conifer forest canopy. Can. J. Rem. Sens. 29(5), 527-535.

Riegl, 2007. Rianalyze 560 for full waveform analysis. Riegl software documentation (www.riegl.com), 46 p.

Rowell, E., Seielstad, C., Vierling, L., Queen, L., Shepperd, W., 2006. Using laser altimetry-based segmentation to refine automated tree identification in managed forests of the black hills, South Dakota. Photogramm. Eng. Remote Sens. 72,1379-1388.

Sithole, G., Vosselman, G., 2004. Experimental comparison of filter algorithms for bare-Earth extraction from airborne laser scanning point clouds. . ISPRS J. Photogramm. Remote Sens. 59, 85-101.

Solberg, S., Næsset, E., Bollandsas, O.M., 2006. Single Tree Segmentation Using Airborne Laser Scanner Data in a Structurally Heterogeneous Spruce Forest. Photogramm. Eng. Remote Sens.12, 1369-1378.

Takahashi, T., Yamamoto, K., Senda, Y., Tsuzuku, M., 2005. Estimating individual tree heights of sugi (Cryptomeria japonica D. Don) plantations in mountainous areas using small-footprint airborne lidar. J. For. Res. 10, 135-142.

Author-produced version of the article published in International Journal of Applied Earth Observation and Geoinformation, 2011, 13(4), 646-656.
The original publication is available at http://www.elsevier.com
DOI: 10.1016/j.jag.2011.04.002

Wagner, W., Ullrich, A., Ducic, V., Melzer, T.,Studnicka, N., 2006. Gaussian decomposition and calibration of a novel small-footprint full-waveform digitising airborne laser scanner. ISPRS J. Photogramm. Remote Sens. 60(2), 100-112.

Author produced version of the article published in International Journal of Applied Earth Observation and Geoinformation, 2011, 13(4), 646-656.
The original publication is available at http://www.elsevier.com
DOI: 10.1016/j.jag.2011.04.002

Figure captions list

Fig. 1: 3D view of the study site.

Fig. 2: Workflow of the proposed segmentation method (i and j are iteration variables used to control Gaussian smoothing and crown fusion respectively).

Fig. 3: Position of the constraining pixels according to the measurement direction.

Fig. 4: Variation of the structural parameter according to field measured plot density (N=12).

Fig. 5: Subset (66 m x 56 m) of the CSM before (left) and after (right) hole-filling. Numbered squares show examples of correction using 8-connected pixels (1), and 4 connected pixels (2: oblique cross, 3-4: vertical cross).

Fig. 6: Examples of tree crown segmentation for 3 plots of varying densities. Crowns are displayed depending on the Gaussian run in which they were extracted. Crosses represent the position of the extracted local maxima. Dots represent the field stem positions according to their dbh classes (small, medium, large).

Fig. 7: Performance of the crown detection according to plot density. Symbols represented the optimized number of Gaussian runs (N = 25). Color scale indicated the dominant dbh class (white: small; grey: medium; black: large) and labels the GC index.

Fig. 8: Field versus Lidar measured tree height (m) (N = 245) according to slope classes.

Fig. 9: Difference between field-derived and lidar-derived tree height on steep slope.

Author-produced version of the article published in International Journal of Applied Earth Observation and Geoinformation, 2011, 13(4), 646-656.
The original publication is available at http://www.elsevier.com
DOI: 10.1016/j.jag.2011.04.002

Figure 1

Click here to download high resolution image

Author-produced version of the article published in International Journal of Applied Earth Observation and Geoinformation, 2011, 13(4), 646-656.
The original publication is available at http://www.elsevier.com
DOI: 10.1016/j.jag.2011.04.002

Figure 2

Click here to download high resolution image

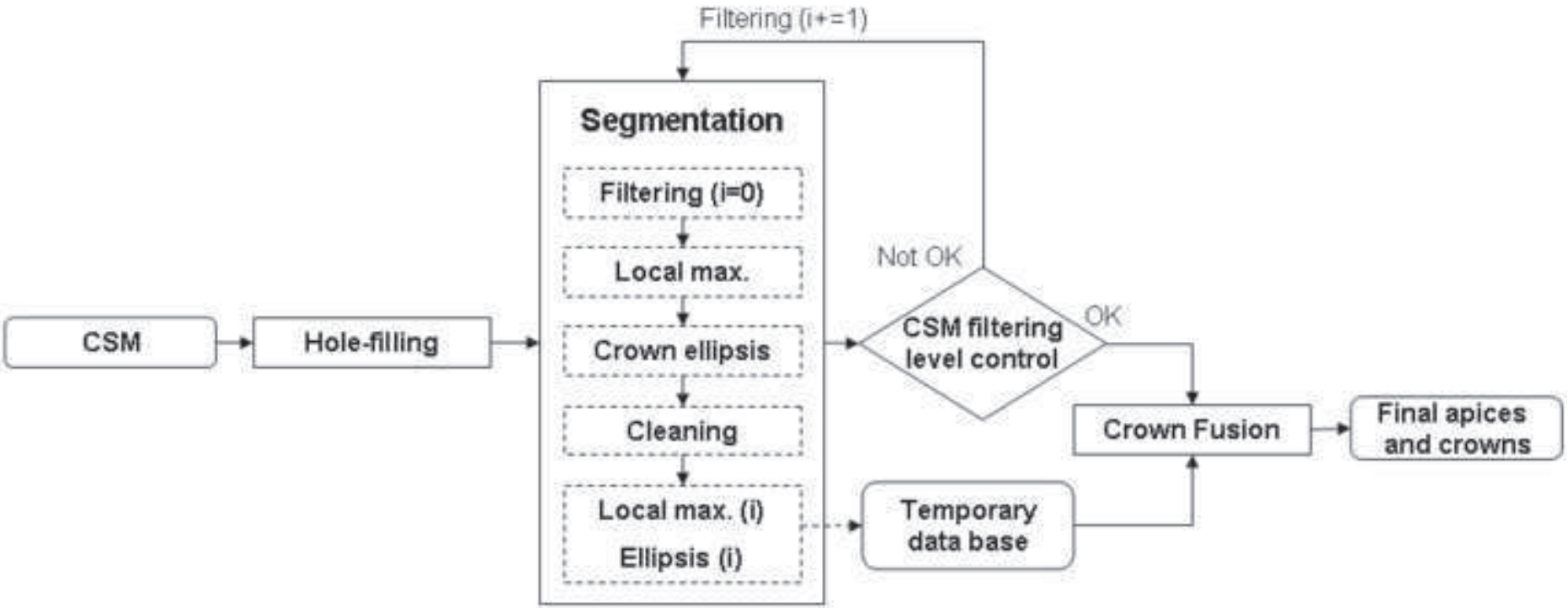

Author-produced version of the article published in International Journal of Applied Earth Observation and Geoinformation, 2011, 13(4), 646-656.
The original publication is available at http://www.elsevier.com
DOI: 10.1016/j.jag.2011.04.002

Figure 3
Click here to download high resolution image

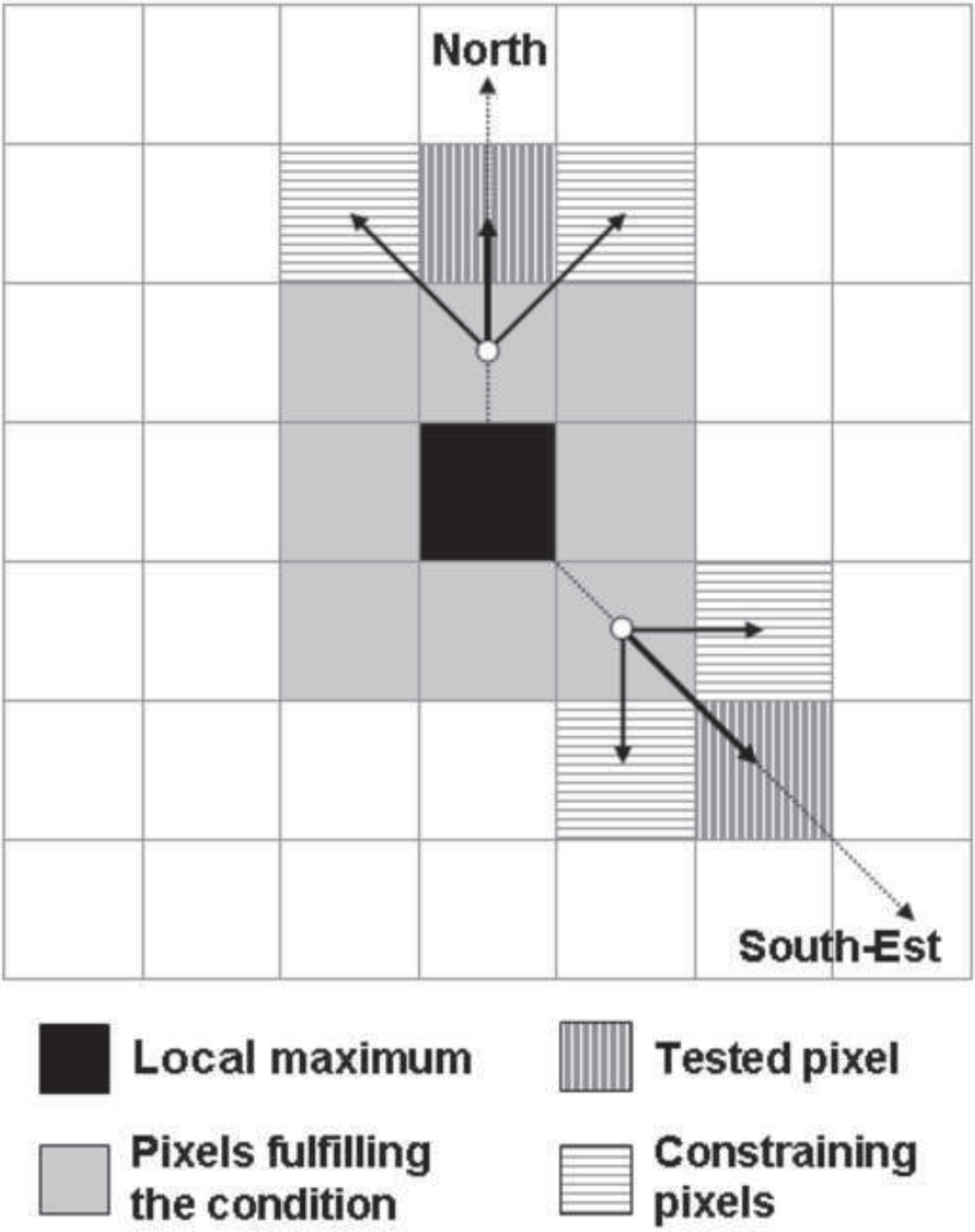

Author-produced version of the article published in International Journal of Applied Earth Observation and Geoinformation, 2011, 13(4), 646-656.
The original publication is available at http://www.elsevier.com
DOI: 10.1016/j.jag.2011.04.002

Figure 4

Click here to download high resolution image

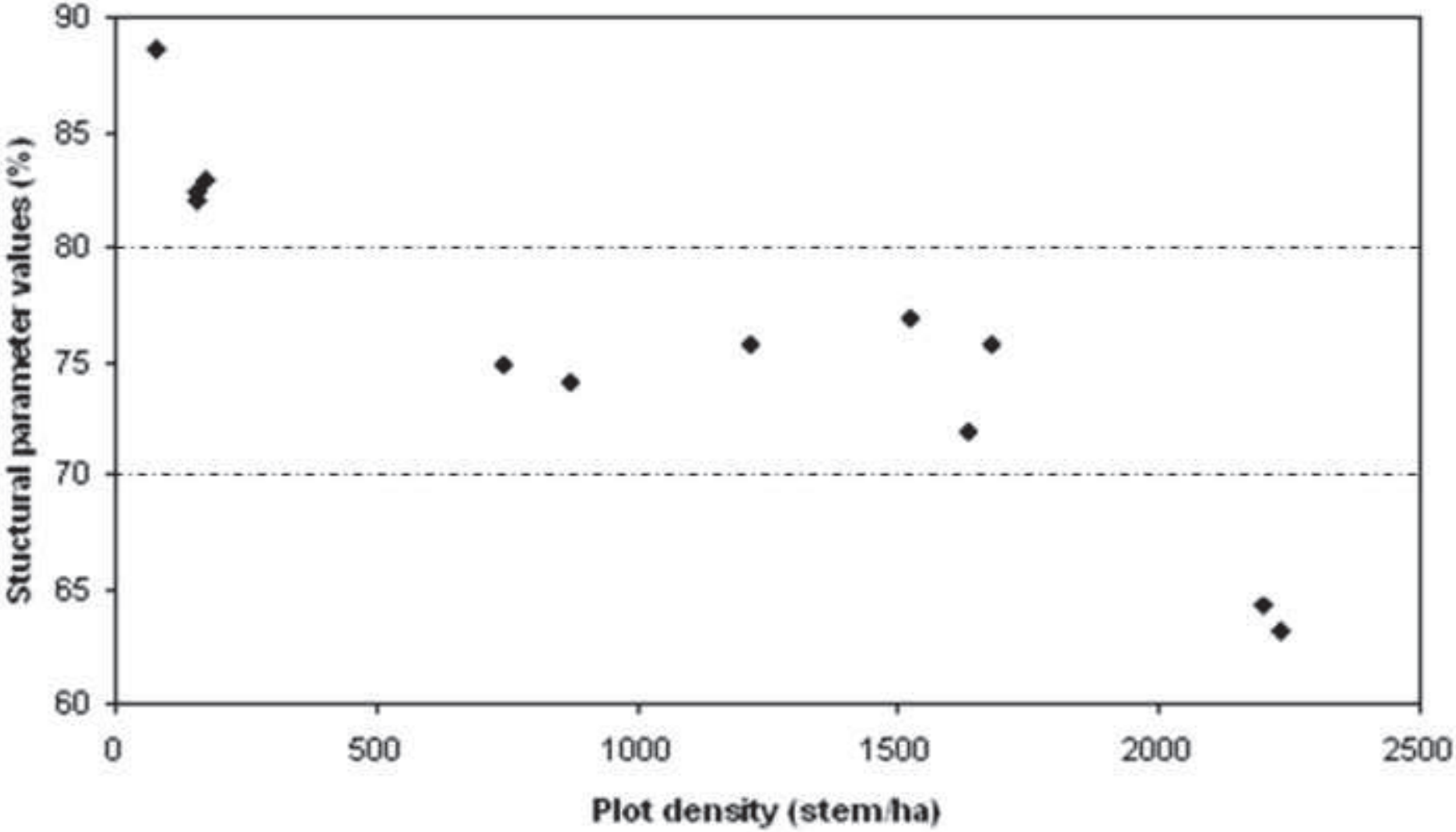

Author-produced version of the article published in International Journal of Applied Earth Observation and Geoinformation, 2011, 13(4), 646-656.
The original publication is available at http://www.elsevier.com
DOI: 10.1016/j.jag.2011.04.002

Figure 5

Click here to download high resolution image

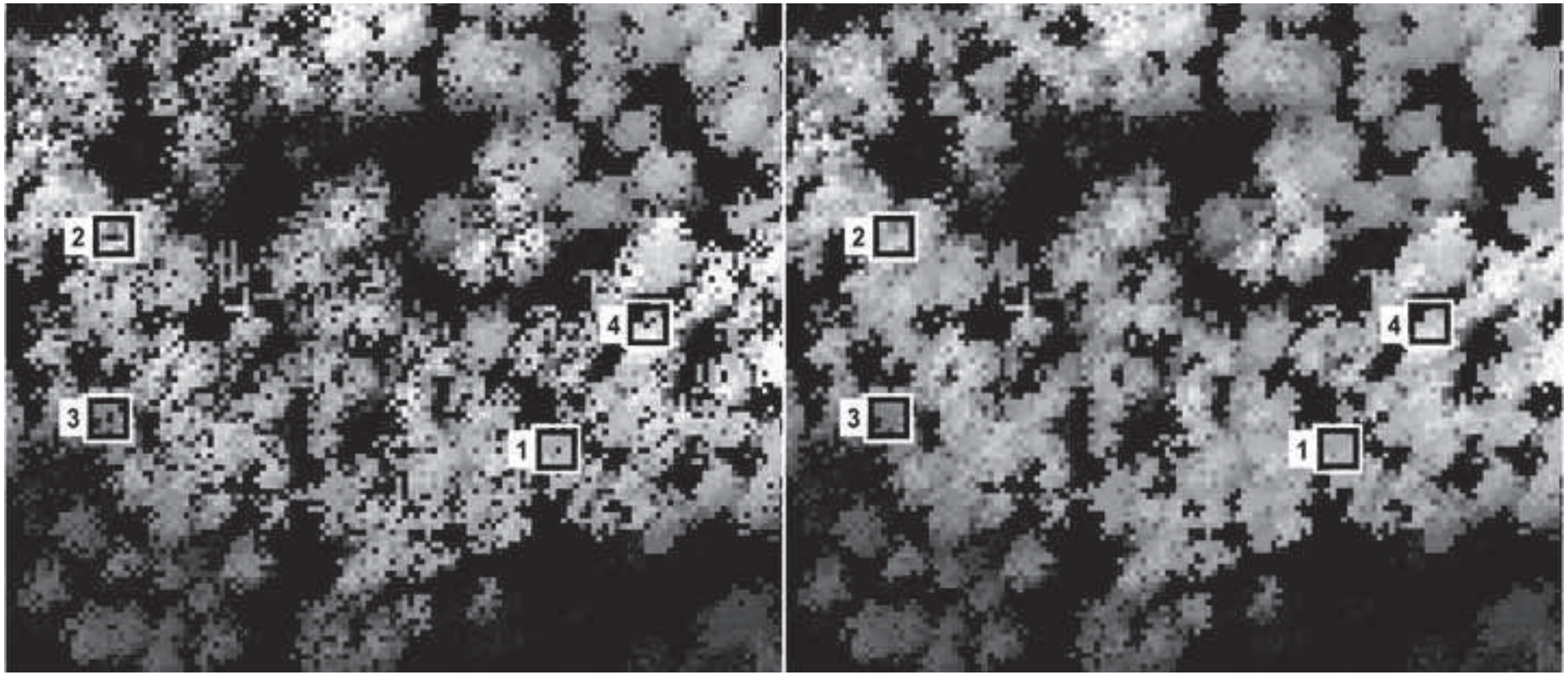

Author-produced version of the article published in International Journal of Applied Earth Observation and Geoinformation, 2011, 13(4), 646-656.
The original publication is available at http://www.elsevier.com
DOI: 10.1016/j.jag.2011.04.002

Figure 6

Click here to download high resolution image

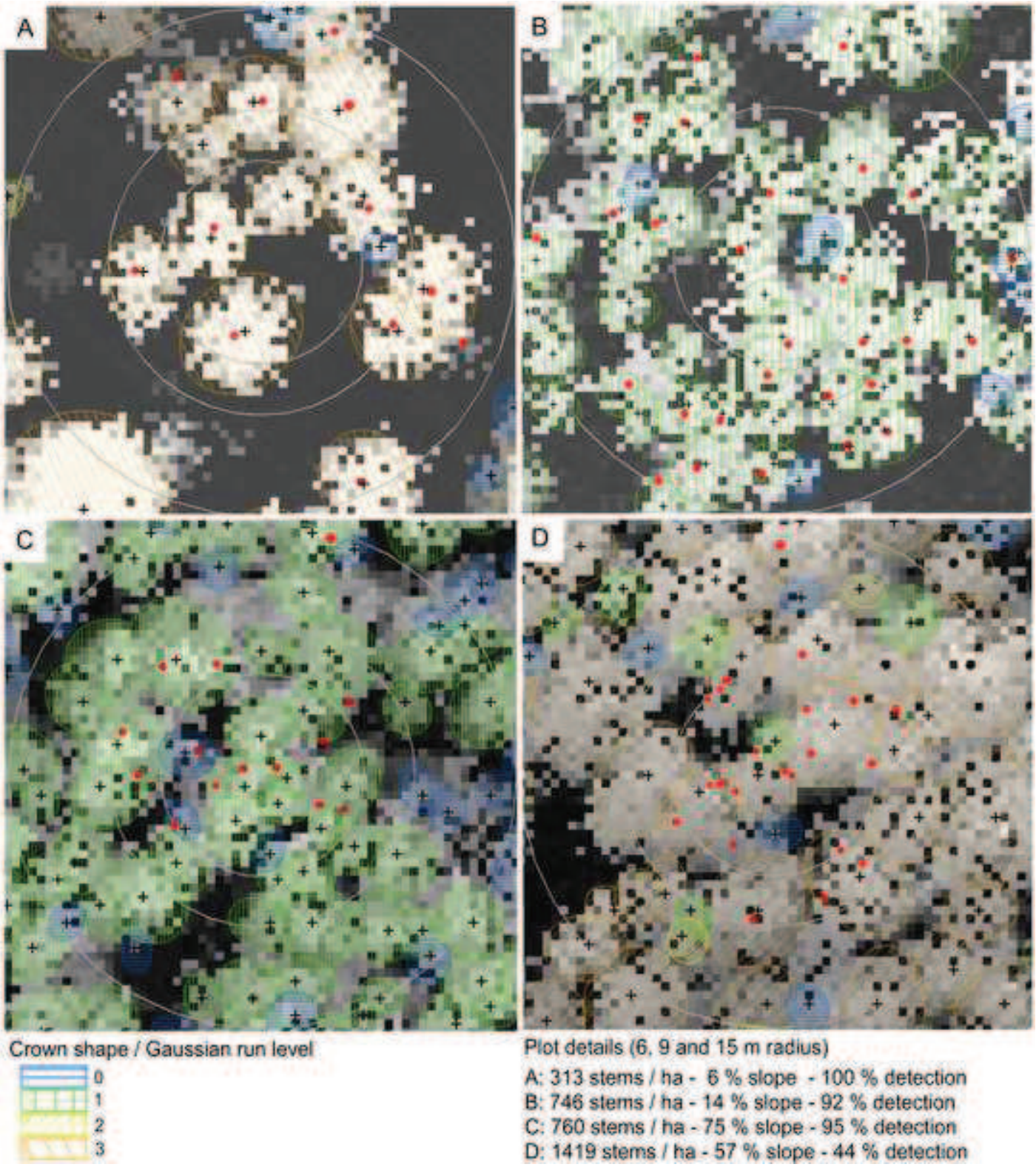

Author-produced version of the article published in International Journal of Applied Earth Observation and Geoinformation, 2011, 13(4), 646-656.
The original publication is available at http://www.elsevier.com
DOI: 10.1016/j.jag.2011.04.002

Figure 7

Click here to download high resolution image

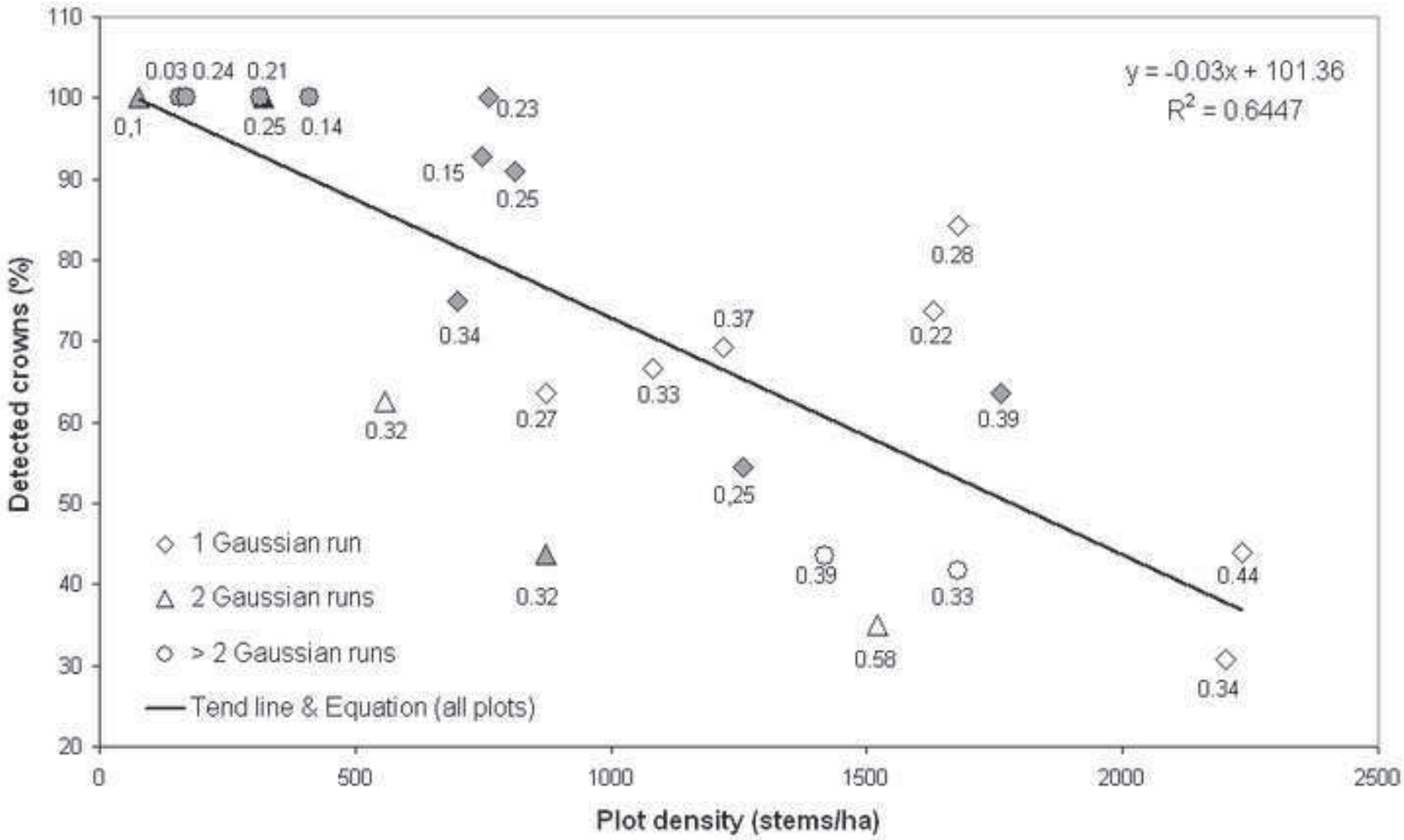

Author-produced version of the article published in International Journal of Applied Earth Observation and Geoinformation, 2011, 13(4), 646-656.
The original publication is available at http://www.elsevier.com
DOI: 10.1016/j.jag.2011.04.002

Figure 8

Click here to download high resolution image

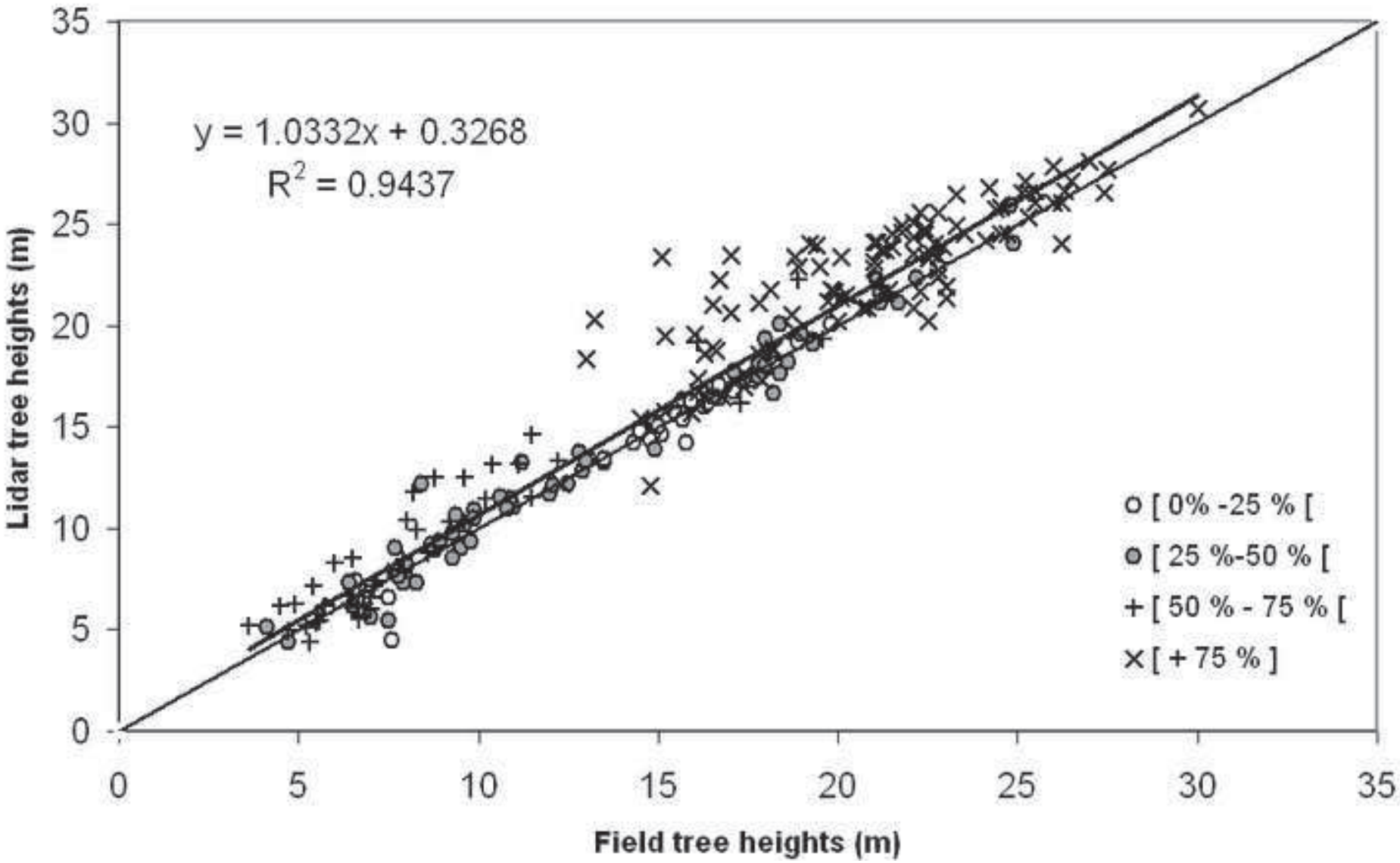

Author-produced version of the article published in International Journal of Applied Earth Observation and Geoinformation, 2011, 13(4), 646-656.
The original publication is available at http://www.elsevier.com
DOI: 10.1016/j.jag.2011.04.002

Figure 9
Click here to download high resolution image

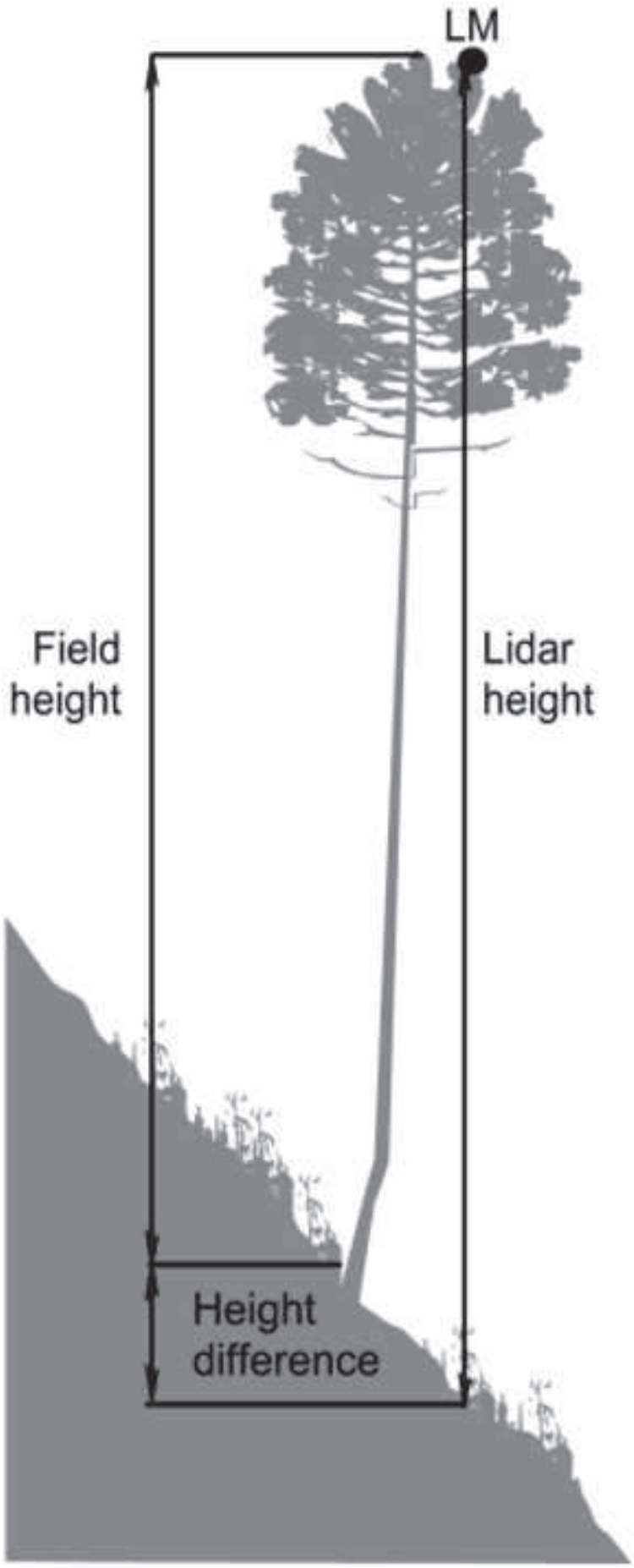

Author-produced version of the article published in International Journal of Applied Earth Observation and Geoinformation, 2011, 13(4), 646-656.
The original publication is available at http://www.elsevier.com
DOI: 10.1016/j.jag.2011.04.002

Table 1

Descriptive statistics of the mean plot values field inventory data (N=25). Note that statistics were computed according to the IFN protocol.

	Density (stem/ha)	Dbh (cm)	Height (m)	*GC*
Minimum	78.59	12.34	5.86	0.03
Mean	960	23,62	14.54	0.28
Median	874.36	24.03	16.35	0.27
Maximum	2234.45	37.48	23	0.58
Standard Deviation	632.55	6.93	5.11	0.12

Author-produced version of the article published in International Journal of Applied Earth Observation and Geoinformation, 2011, 13(4), 646-656.
The original publication is available at http://www.elsevier.com
DOI: 10.1016/j.jag.2011.04.002

Table 2

Threshold parameter values used to constrain the segmentation

Structural parameter	> 80	<=80 and =>70	< 70
Segmentation parameter	0.98	0.85	0.8

Author-produced version of the article published in International Journal of Applied Earth Observation and Geoinformation, 2011, 13(4), 646-656.
The original publication is available at http://www.elsevier.com
DOI: 10.1016/j.jag.2011.04.002

Table 3

Statistics of the segmentation parameters for the 25 plots

	Nb of Gaussian filter runs	Nb LM/Crown	Crowns from optimized filtering	Crowns from lower filtering levels
Min	1	1	50	0
Mean	1.8	1.12	90.28	9.72
Max	4	1.37	100	50
SD	0.96	0.12	11.12	11.12

Author-produced version of the article published in International Journal of Applied Earth Observation and Geoinformation, 2011, 13(4), 646-656.
The original publication is available at http://www.elsevier.com
DOI: 10.1016/j.jag.2011.04.002

Table 4

This table presents results of the segmentation performance for the 25 field plots. Note that commission errors were evaluated within a 6 m radius from the plot centre.

Diameter class		All	Large	Medium	Small
Nb of stems		391	32	156	203
Detection (%)	Min	30.76	80	14	0
	Mean	73.97	98.18	92.63	45.66
	Max	100	100	100	100
	SD	23.66	6.03	11.61	34.41
Omission (%)	Min	0	0	0	0
	Mean	21.02	1.81	6.54	54.33
	Max	69.23	20	36.36	100
	SD	23.66	6.03	11.61	34.41
Commission (%) (6 m radius)	Min	0	-	-	-
	Mean	5.91	-	-	-
	Max	25	-	-	-
	SD	8.41	-	-	-

Author-produced version of the article published in International Journal of Applied Earth Observation and Geoinformation, 2011, 13(4), 646-656.
The original publication is available at http://www.elsevier.com
DOI: 10.1016/j.jag.2011.04.002

Table 5

Differences between lidar and field measurements (ΔH = field – lidar) for the 245 identified trees (**N_{Stem}**). Statistics are reported for all trees, dbh classes and terrain slope classes.

dbh classes (cm)		All		Large		Medium		Small	
				[34.7 – α [		**[22.44 – 34.7 [**		**[7.48 – 22.44 [**	
		ΔH	|ΔH|	ΔH	|ΔH|	ΔH	|ΔH|	ΔH	|ΔH|
	N_{Stem}	245	245	29	29	130	130	86	86
	Mean (m)	-0.84	1.23	-1.30	1.37	-0.83	1.19	-0.70	1.22
	Min (m)	-8.26	0	-4.57	0.07	-6.48	0	-8.26	0.02
	max (m)	3.16	8.26	0.85	4.57	2.24	6.48	3.16	8.26
	SD (m)	1.63	1.36	1.24	1.15	1.51	1.24	1.89	1.59
	RMSE (m)	1.83	-	1.78		1.72		2.00	
slope classes (%)		<=25		>25 & <=50		>50 & <=75		>75	
		ΔH	|ΔH|	ΔH	|ΔH|	ΔH	|ΔH|	ΔH	|ΔH|
	N	40	40	54	54	51	51	100	100
	Mean (m)	0.10	0.38	-0.18	0.72	-0.83	1.13	-1.58	1.88
	Min(m)	-0.78	0.03	-3.8	0.02	-3.7	0.02	-8.26	0
	max(m)	3.16	3.16	2.04	3.8	1.15	3.7	2.72	8.26
	SD (m)	0.65	0.53	0.96	0.66	1.31	1.06	1.95	1.67
	RMSE (m)	0.65		0.97		1.54		2.50	

Author-produced version of the article published in International Journal of Applied Earth Observation and Geoinformation, 2011, 13(4), 646-656.
The original publication is available at http://www.elsevier.com
DOI: 10.1016/j.jag.2011.04.002

Table 6

Evaluation of the lidar derived crown diameters ($\mathbf{N_{Crown}}$ = 53): difference between ground truth and lidar-derived values. NS and EW represent the North-South and the East-West directions respectively. The Mean Diameter is the mean of the two later values.

	All directions			North-South			Est-West		
	All	Plot 1	Plot 2	All	Plot 1	Plot 2	All	Plot 1	Plot 2
Min	-2.08	-0.68	-2.08	-1.36	-0.68	-1.36	-2.08	-0.48	-2.08
Mean (m)	0.95	0.79	1.00	1.19	0.62	1.37	0.72	0.96	0.63
Mean (%)	17.46	12.34	19.11	21.90	11.53	25.26	13.02	13.15	12.97
Max	6.02	2.84	6.02	6.02	2.48	6.02	2.84	2.84	2.66
SD	1.14	0.88	1.21	1.18	0.77	1.23	1.07	0.98	1.09
RMSE	1.48	1.17	1.57	1.66	0.97	1.83	1.27	1.34	1.25